Inorganic Chemistry

Article

pubs.acs.org/IC

Solid-State Structure of a Degradation Product Frequently Observed on Historic Metal Objects

Robert E. Dinnebier,*[,†] Tomče Runčevski,[†] Andrea Fischer,[‡] and Gerhard Eggert[‡]

[†]Max-Planck-Institute for Solid State Research, Heisenbergstrasse 1, 70569 Stuttgart, Germany

[‡]State Academy of Art and Design Stuttgart, Am Weißenhof 1, 70191 Stuttgart, Germany

Supporting Information

ABSTRACT: In the course of the investigation of glass-induced metal corrosion processes, a microcrystalline sodium copper formate hydroxide oxide hydrate, $Cu_4Na_4O(HCOO)_8(H_2O)_4(OH)_2$, was detected on a series of antique works of art, and its crystal structure was determined ab initio from high-resolution laboratory X-ray powder diffraction data using the method of charge flipping, simulated annealing, and difference-Fourier analysis ($P4_2/n$, a = 8.425 109(97) Å, c = 17.479 62(29) Å, V = 1240.747(35) Å^3, Z = 8). In the crystal structure, the metal cations are interconnected in a two-dimensional metal−organic framework via the oxygen atoms of the formate, hydroxide, and oxide anions. Doublets of face-sharing square pyramidal Cu^{2+} polyhedra are linked via a single, central oxide oxygen atom to give a paddle-wheel arrangement, while the Na^+ cations are organized in Na_2O_{11} moieties with highly disordered, edge-sharing octahedral coordination. In addition, hydrogen bonding plays an important role in stabilizing the crystal structure.

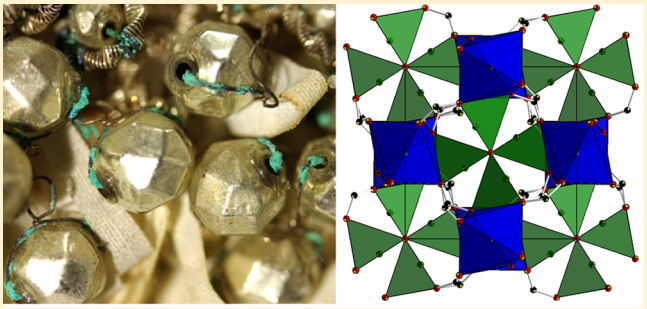

1. INTRODUCTION

A significant number of historic glass and enamel objects in museum collections suffer by a degradation phenomenon recently characterized as "glass-induced metal corrosion".[1,2] Bright blue-green and green corrosion products are formed at the interface of metal (copper alloys) and glass. Two contributing factors are involved in this corrosion process. First, the chemical instability of the glass, which results in the development of liquid alkaline films on the glass surface, and second, the exposure to carbonyl pollutants (formaldehyde and formic and acetic acids) emitted by wood, wood products, and other construction materials. To clarify the cause of damage in detail, corrosion products of more than 200 affected objects were investigated (a selection of three is given in Figure 1a−c). On every second object the compound sodium copper formate hydroxide oxide hydrate, $Cu_4Na_4O(HCOO)_8(H_2O)_4(OH)_2$ (**Corr1**), was identified by Raman spectroscopy. Among the other compounds detected were $Cu_2(OH)_3HCOO$, $Na_2[Cu(CO_3)_2]\cdot 3H_2O$ (known as the mineral chalconatronite), and different acetates. **Corr1** was reported in the literature by Trentelman et al.[3] as a "pale blue corrosion product" occurring on copper alloy artifacts (without glass). Sodium-containing soils and conservation treatments in soda solutions were mentioned as possible sources for alkali metal ions in its formation. So far, no details on the solid-state structure of **Corr1** have been presented in the literature. Its high prevalence as one of the main corrosion products of many important artifacts motivated us to investigate its solid-state chemistry further and to provide the community with its detailed crystal structure.

Field emission scanning electron microscopy (FE-SEM) images, taken on affected artifacts, showed that **Corr1** crystallizes in the form of thin tabular microcrystals with an edge length of ∼1−2 μm (Figure 1d). Since our attempts to grow single crystals of quality suitable to single-crystal diffraction failed, the crystal structure of **Corr1** was solved and refined from high-resolution laboratory X-ray powder diffraction (XRPD) data. It was found that the metal cations are connected through organic ligands and hydroxide anions to form an extended two-dimensional metal−organic framework (MOF) structure. MOF compounds, in their crystal structures, combine organic and inorganic building blocks to give hybrid structures with a plethora of interesting properties.[4−9]

To learn more about the degradation processes related to the glass-induced metal corrosion, various laboratory tests were performed. Moreover, a synthetic route of **Corr1** was derived. As mentioned above, the crystal structure of **Corr1** was detailed from XRPD data, and it was shown that it can be used in executing routine, fast, and nondestructive quantitative phase analyses on artifact samples, which is of relevance to conservation investigations. Herein, we report on those findings.

Received: November 21, 2014
Published: February 24, 2015

DOI: 10.1021/ic5027637
Inorg. Chem. 2015, 54, 2638−2642

Figure 1. (a) Glass beads on a traditional Black Forest headdress (late 19th century) from the Franziskanermuseum Villingen Schwenningen (Germany). (b) Earring (early 20th century) from the Museum für Hamburgische Geschichte (Germany). (c) Detail of a Double-Triptych, painted enamel on copper (Limoges, 16th century), Copyright the Frick Collection, New York. (d) Field emission scanning electron microscopy image of **Corr1**.

2. EXPERIMENTAL SECTION

Elemental Analysis. The chemical composition of corrosion samples was analyzed by an energy-dispersive X-ray (EDX) system (Noran, Vantage System). The main elements found were O, Na, and Cu with relative abundances given in Table 1. Note that the differences within the compositions of the samples studied are due to the presence of different, small amounts of impurities, which also occur as degradation products.

Table 1. Elemental Analysis of Corrosion Products

sample	O[a]	Na[a]	Cu[a]
1	64.9	15.8	19.3
2	69.6	16.8	13.6
3[b]	65.0	15.4	18.9

[a]Normalized values to 100%. [b]In sample 3, small amounts of S (0.34) and K (0.37) were detected.

Pattern Collection and Indexing, Crystal Structure Solution, and Rietveld Refinement. High-resolution XRPD pattern of **Corr1** (Figure 2) was collected at room temperature on a high-resolution laboratory powder diffractometer in transmission mode using a Stoe Stadi-P transmission diffractometer (primary beam Johann-type Ge monochromator for Cu $K\alpha_1$-radiation) with the sample distributed between two thin X-ray transparent kapton foils. The sample was not pretreated, except of careful manual powdering in an agate mortar. The powder pattern of **Corr1** was recorded for 20 h in the range from 5 to 85° 2θ with a step width of 0.015° 2θ using a linear position sensitive silicon strip detector (Mythen-Dectris) with an opening of ~12° 2θ (further details are given in Table 2). The sample was rotated during the data collection for better particle statistics.

For indexing of the powder pattern of **Corr1**, the program TOPAS Version 4.1 (Bruker-AXS, 2007) was used.[10] Indexing was performed by iterative use of singular value decomposition (LSI),[11] leading to a primitive tetragonal unit cell with lattice parameters given in Table 2. The most probable space group was determined to be $P4_2/n$ (No. 86) from the observed extinction rules. The number of formula units per unit cell was estimated to be $Z = 8$ from volume increments. The peak profiles and precise lattice parameters of the powder pattern were determined by a Pawley fit[12] using the fundamental parameter (FP) approach.[13] For the modeling of the background, Chebychev polynomials of higher order were employed. The refinement converged quickly. The structure determination of **Corr1** was performed in the space group $P4_2/n$ by the method of Charge Flipping[14] supported by the inclusion of the tangent formula.[15] The positions of most of the atoms were found in less than a minute. By visual inspection falsely assigned atom types were detected and corrected. The atomic positions of all missing non-hydrogen atoms (mainly the carbon atoms of the formate groups) were found by the global optimization method of simulated annealing[16] and inspecting the difference-Fourier maps.

The structure was validated by unrestrained Rietveld refinement (Figure 2).[17] The thermal displacement factors were freely refined. The positions of the hydrogen atoms were calculated by the program suite Mercury CSD 3.3.[18] Agreement factors are listed in Table 2. The

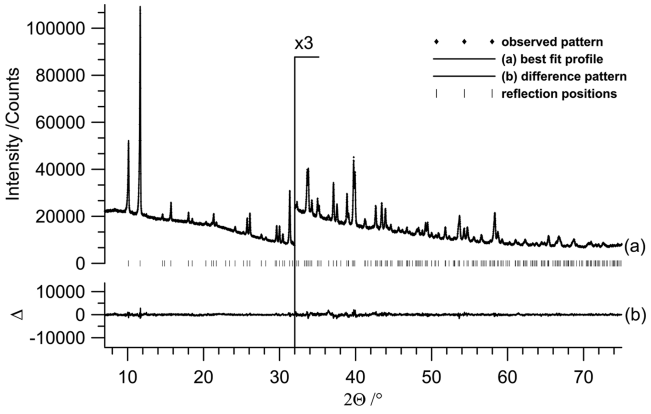

Figure 2. Scattered X-ray intensities of **Corr1** at ambient conditions, as a function of diffraction angle. The observed pattern (diamonds) measured in Debye–Scherrer geometry, the best Rietveld fit profiles (line), and the difference curve between the observed and the calculated profiles (below) are shown. The high angle part is enlarged for clarity.

Table 2. Selected Crystallographic and Rietveld Refinement Details of Powder Diffraction Experiment Performed on Corr1

compound name	**Corr1**
molecular formula	$Cu_4Na_4O(HCOO)_8(H_2O)_4(OH)_2$
sum formula	$Cu_4Na_4O_{23}C_8H_{26}$
formula weight (g/mol)	414.18
crystal system	tetragonal
space group	$P4_2/n$ (No. 86)
Z	8
a/Å	8.425 109(97)
c/Å	17.479 62(29)
V/Å^3	1240.747(35)
temperature (K)	298
ρ (calcd) (g cm^{-3})	2.255
wavelength (Å)	1.540 59
R-exp (%)	1.042
R-p (%)	1.259
R-wp (%)	1.662
R-Bragg (%)	0.549
starting angle (deg 2θ)	5.0
final angle (deg 2θ)	75.0
step width (deg 2θ)	0.015
time/scan (h)	20
no. of variables	70

DOI: 10.1021/ic5027637
Inorg. Chem. 2015, 54, 2638–2642

atomic coordinates are given in the CIF file in the Supporting Information. The crystallographic data were deposited at ICSD. Crystal voids were calculated with the program Crystal Explorer.[19]

Raman Spectroscopy. The micro-Raman spectra were recorded by using a Renishaw inVia Raman spectrometer (grating 1800 L/mm, resolution 1 cm^{-1}) equipped with a Leica DMLM microscope and a RenCam CCD detector. The spectra were taken from 100 to 3700 cm^{-1}, using a He−Ne laser operating at 632.8 nm. The power of the laser was less than 400 μW focused into a 0.7 μm spot through a 50× microscope objective.

Scanning Electron Microscopy. The FE-SEM images were obtained using a Zeiss SUPRA 40 VP Microscope (accelerated voltage 10 kV, SE detector).

3. RESULTS AND DISCUSION

Synthesis. To better understand the glass-induced metal corrosion processes we attempted to derive a synthetic route to produce **Corr1**. Synthetic $Na_2Cu(CO_3)_2{\cdot}3H_2O$ (mineral name: chalconatronite) was used as a starting reactant. The compound was stored in a desiccator with formaldehyde/formic acid-rich atmosphere (ca. 200 ppm each, 75% relative humidity) for reaction. In a period of ∼six months **Corr1** was obtained as a product. The chemical composition and crystal structure of the synthesized product were confirmed by a Rietveld refinement.

Crystal Structure Description. The crystal structure of **Corr1** was solved from XRPD data collected from affected artifacts providing the corrosion product in pure phase. The crystal packing of the compound is shown in Figure 3, where it can be seen that **Corr1** is composed of MOF layers, packed perpendicularly to the *c*-crystallographic axis. **Corr1** crystallizes in the tetragonal $P4_2/n$ space group, with the Cu^{2+} cation placed on a general position (with site multiplicity 8) and two Na^+ cations placed on special positions with multiplicity 4. The metal cations are interconnected in a two-dimensional MOF structure via the oxygen atoms of the formate, hydroxide, and oxide anions.

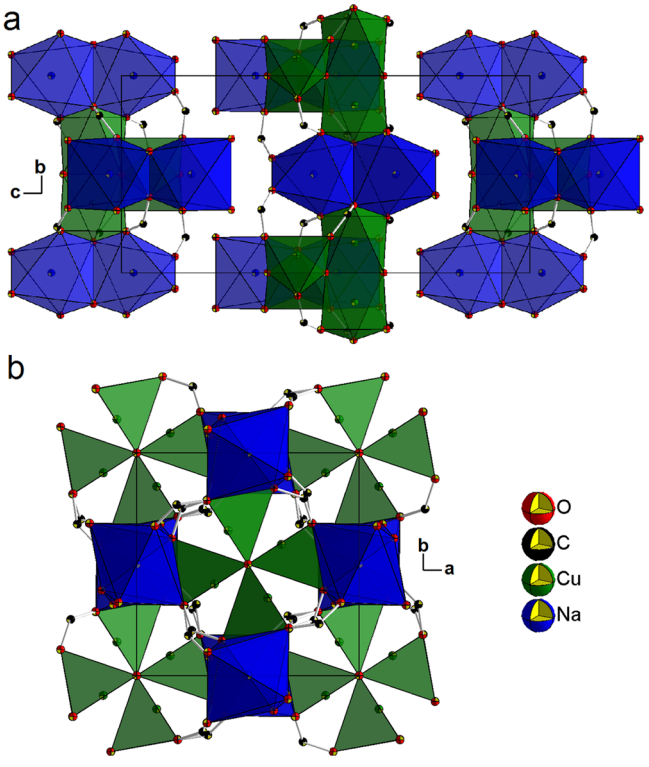

Figure 3. Crystal packing diagrams of **Corr1**, presented in the direction of (a) the *a*-crystallographic axis and (b) the *c*-crystallographic axis.

The coordination oxygen atoms around the Cu^{2+} cations form an elongated square pyramid (Figure 4a). Doublets of face-sharing square pyramidal Cu^{2+} polyhedra are linked via a single, central oxide oxygen atom (O6) to give a paddle-wheel arrangement. The Cu−O bond lengths are listed in Table 3.

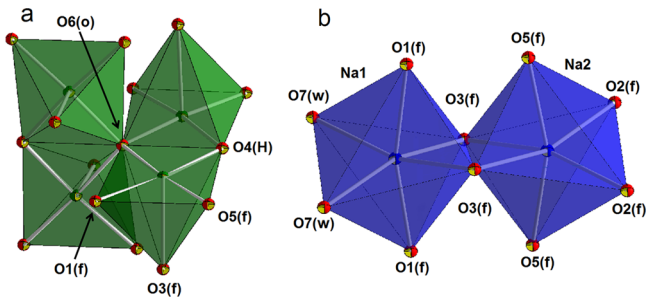

Figure 4. (a) Elongated square pyramidal Cu^{2+} polyhedra, running in a paddle-wheel fashion. (b) Edge-sharing, distorted Na^+ octahedra forming Na_2O_{11} units. Abbreviations: o = oxide, f = formate, H = hydroxide, w = water.

Table 3. Selected Bond Lengths and Atom Contacts in the Solid-State Structure of Corr1

atom−atom	length, Å	atom−atom	length, Å
Cu1−O1	1.942(10)	Na1−O7 (×2)	2.452(10)
Cu1−O4	1.919(10)	Na2−O3 (×2)	2.400(10)
Cu1−O5	2.014(10)	Na2−O2 (×2)	2.386(10)
Cu1−O6	1.930(10)	Na2−O5 (×2)	2.327(10)
Cu1−O3	2.364(10)	hydrogen bonding	
Na1−O1 (×2)	2.393(10)	O7···O2	2.875(10)
Na1−O3 (×2)	2.465(10)	O7···O7	2.779(10)

The Na^+ cations are organized in Na_2O_{11} moieties with highly disordered, edge-sharing octahedral coordination, as seen in Figure 4b. Selected bond lengths are given in Table 3. One of the Na^+ cations (Na2) is fully coordinated by oxygen atoms from the formate anions, which are bridging it with neighboring Na^+ and Cu^{2+} cations. The other Na^+ cation (Na1) is surrounded by the oxygen atoms of four formates and two water molecules. These water molecules play an important role in stabilizing the crystal structure, done via the formation of an interlayer hydrogen-bonding network. Namely, very short contacts within the water molecules from neighboring layers and within the water molecules and the formate anions are detected, indicating a relatively strong hydrogen-bonding network (Table 3).

The solid-state structure of **Corr1** is characterized by the presence of crystal voids inside the two-dimensional MOF layers, which are further surrounded by the hydrogen-bonding network. The 0.002 au smoothed surface gave a void space of 5.22% (relative to the unit cell volume), as shown in Figure 5.

There are reports on crystal growth of MOFs onto different inorganic matrices.[20−22] The growth of **Corr1** on metals is naturally occurring example, and further structural and kinetics examinations can provide useful hints for crystal growth approaches of MOF materials.

Quantitative Phase Analysis. In heritage conservation, identification of corrosion products plays a crucial role. XRPD

DOI: 10.1021/ic5027637
Inorg. Chem. 2015, 54, 2638−2642

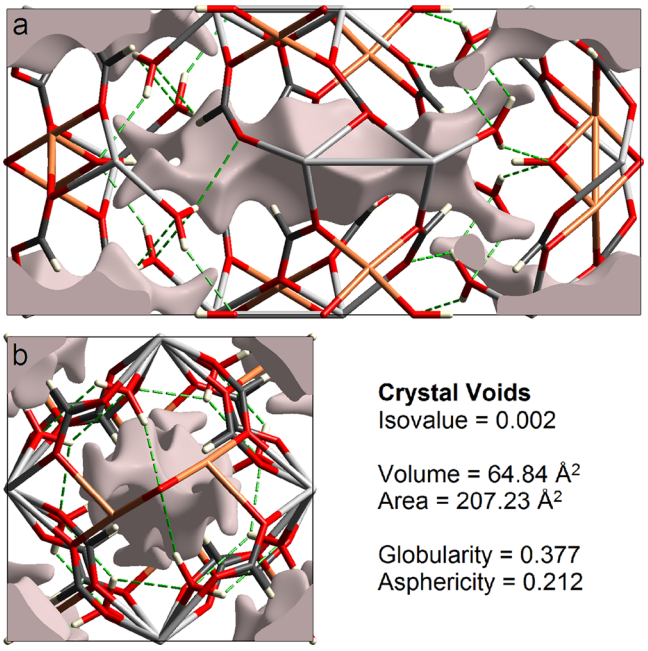

Figure 5. Crystal voids in the solid-state structure of **Corr1**. The isovalue was set to 0.002 au. Projections perpendicular to the (a) *a*-crystallographic and (b) *c*-crystallographic axes. (inset) The statistics of the calculation. (Color code: gray = sodium, orange = copper, red = oxygen, black = carbon and white = hydrogen.).

is a prefect technique for that kind of analysis, as it is a nondestructive, fast, and easy-to-use method. The XRPD data can be used in routine qualitative analysis, owing to the fact that the powder pattern is a fingerprint signature to the corresponding crystal structure. The biggest advantage of XRPD, however, is the ability of performing simultaneous qualitative and quantitative analyses of crystalline constituents in mixtures, by using the Rietveld refinement method.[17] Moreover, the presence of amorphous content can be detected, and the amount of this content can be estimated. This procedure requires knowledge of every crystal structure present in the mixture that is a subject of investigation.

Corr1 was very frequently detected as a corrosion product; thus, solving its crystal structure stood as a high priority. The solution of its structure reported in this article makes many artifacts amenable to (qualitative and) quantitative phase Rietveld analyses. As a showcase, Figure 6 presents the Rietveld refinement plot of a corrosion mixture formed on a museum's artifact that was randomly selected for testing. The data were collected on a laboratory diffractometer for a few hours. The sample was placed on a plate and rotated during data collection. The main constituents of the mixture were readily found to be **Corr1**, $Cu_2(OH)_3HCOO$, and Cu_2O with relative amounts of 79.2(1) %, 19.5(1) %, and 1.3(1) %, respectively.

Raman Spectroscopy. Figure 7 presents the Raman spectrum of blue-green **Corr1** crystals collected from a traditional Black Forest headdress (Figure 1a). The Raman band frequencies and relative intensities are in agreement with those of the published data,[3] with exception of the weak band centered at 3540 cm^{-1}. This band was assigned to the hydroxyl stretching vibration and appeared with extremely low intensity in the spectrum presented in Figure 7. (Note that this band was not observed in all of the Raman spectra systematically collected from many artifacts, probably due to its low intensity). Trentelman et al.[3] assigned the bands at 937 and 2960 cm^{-1} to

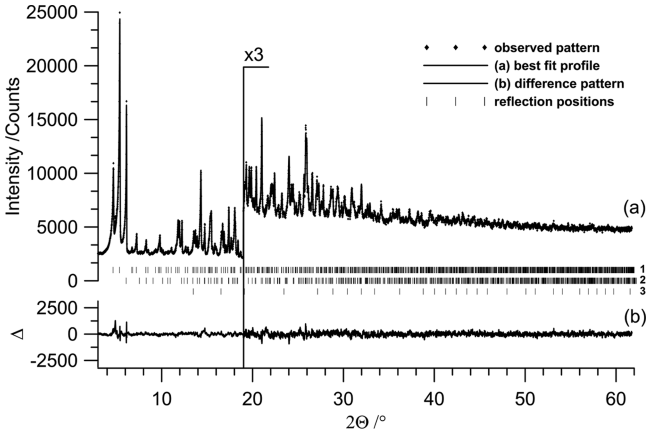

Figure 6. Scattered X-ray intensities of a corrosion mixture at ambient conditions, as a function of diffraction angle. The observed pattern (diamonds) measured in Debye–Scherrer geometry, the best Rietveld fit profiles (line) and the difference curve between the observed and the calculated profiles (below) are shown. The high angle part is enlarged for clarity. The following constituents were identified: **Corr1** (**1**), $Cu_2(OH)_3HCOO$ (2) and Cu_2O (3) with relative amounts of 79.2(1) %, 19.5(1) % and 1.3(1) %, respectively.

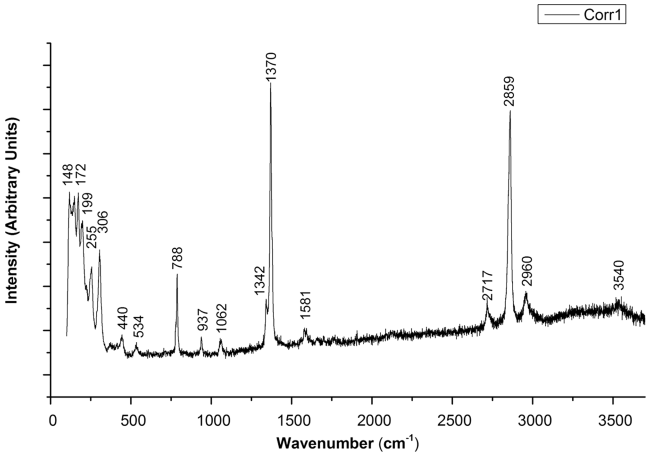

Figure 7. Raman spectrum of blue-green corrosion products from a traditional Black Forest headdress.

acetate vibrations. Since the crystallographic analysis and the synthesis proved the absence of acetate anions, there must be alternative assignments. Kartha and Venkateswaran[23] reported the Raman spectrum of the formate $Yb(HCOO)_2{\cdot}2H_2O$, which has Raman-active C–H stretches at both 2869 and 2966 cm^{-1}.

4. CONCLUSIONS

This article reports on the solid-state structure of sodium copper formate hydroxide oxide hydrate, $Cu_4Na_4O(HCOO)_8(H_2O)_4(OH)_2$, found to be the main product of glass-induced metal corrosion processes of many historic glass and enamel objects in museum collections. The title compound crystallizes in the form of microcrystals with tetragonal symmetry ($P4_2/n$, a = 8.425 109(97) Å, c = 17.479 62(29) Å, V = 1240.747(35) Å^3, Z = x). The crystal packing is characterized by face-sharing square pyramidal Cu^{2+} polyhedra forming a paddle-wheel arrangement and Na_2O_{11} moieties with highly disordered, edge-sharing octahedral coordination. Formate, hydroxide, and oxide oxygen atoms are bridging the metal polyhedral to form a two-dimensional MOF layer. The MOF is interrupted by relatively

DOI: 10.1021/ic5027637
Inorg. Chem. 2015, 54, 2638–2642

large crystal voids, and neighboring layers are communicating via strong hydrogen bonding. This kind of crystal packing makes **Corr1** a possible ion-conductor system. The knowledge of the crystal structure of **Corr1** was found to be of great benefit to conservation science. Namely, by reporting the crystallographic details of this abundant corrosion product, many artifacts became amenable to quantitative and qualitative phase analyses, performed with ease using the XRPD as a nondestructive method.

Corrosion products, in a way, can act as a dosimeter of reactive compounds present in the immediate surrounding air. The analysis of the crystal structure of the frequently detected **Corr1** proved the presence of the formate anion. We assume that the formate originates from wood-based materials and other sources present in display cases.

■ ASSOCIATED CONTENT

Supporting Information

Crystallographic details as CIF file. This material is available free of charge via the Internet at http://pubs.acs.org.

■ AUTHOR INFORMATION

Corresponding Author

*E-mail: r.dinnebier@fkf.mpg.de.

Notes

The authors declare no competing financial interest.

■ ACKNOWLEDGMENTS

The authors gratefully acknowledge Ms. V. Duppel (Max Planck Institute, Stuttgart) for performing the EDX analysis, Mr. D. Kirchner (German Mining Museum, Bochum) for taking the FE-SEM images, and Prof. P. Makreski (Ss. Cyril and Methodius University, Skopje) for valuable discussions on the Raman assignment. Figure 1c is adapted from the Double Tiered Triptych: Scenes from the Passion of Christ (workshop of Nardon Penicaud), Copyright the Frick Collection.

■ REFERENCES

(1) Eggert, G. *Corros. Eng., Sci. Technol.* **2010**, *45*, 414−419.
(2) Eggert, G.; Wollmann, A.; Schwahn, B.; Hustedt-Martens, E.; Barbier, B.; Euler, H. *Proceedings of the ICOM-CC 15th Triennial Conference;* Bridgland, J., Ed.; Allied Publishers: New Delhi, 2008; Vol. *I*, pp 211−216.
(3) Trentelman, K.; Stodulski, L.; Scott, D.; Back, M.; Stock, S.; Strahan, D.; Drews, A. R.; O'Neill, A.; Weber, W. H.; Chen, A.; Garrett, S. *Stud. Conserv.* **2002**, *47*, 217−227.
(4) O'Keeffe, M. *Chem. Soc. Rev.* **2009**, *38*, 1215−1217.
(5) Magdysyuk, O. V.; Denysenko, D.; Weinrauch, I.; Volkmer, D.; Hirscher, H.; Dinnebier, R. E. *Chem. Commun.* **2014**, DOI: 10.1039/c4cc07554d.
(6) Murray, L. J.; Dincă, M.; Long, J. R. *Chem. Soc. Rev.* **2009**, *38*, 1294−1314.
(7) Kurmoo, M. *Chem. Soc. Rev.* **2009**, *38*, 1353−1379.
(8) Allendorf, M. D.; Bauer, C. A.; Bhakta, R. K.; Houk, R. J. T. *Chem. Soc. Rev.* **2009**, *38*, 1330−1352.
(9) Eikeland, E.; Lock, N.; Filsø, M.; Stingaciu, M.; Shen, Y.; Overgaard, J.; Iversen, B. B. *Inorg. Chem.* **2014**, *53*, 10178−10188.
(10) *Topas,* Version 4.1; Bruker AXS: Karlsruhe, Germany, 2007.
(11) Coelho, A. A. *J. Appl. Crystallogr.* **2003**, *36*, 86−95.
(12) Pawley, G. S. *J. Appl. Crystallogr.* **1981**, *14*, 357−361.
(13) Cheary, R. W.; Coelho, A. A.; Cline, J. P. *J. Res. Natl. Inst. Stand. Technol.* **2005**, *109*, 1−25.
(14) Oszlányi, G.; Süto, A. *Acta Crystallogr.* **2004**, *A60*, 134−141.
(15) Karle, J.; Hauptman, H. *Acta Crystallogr.* **1956**, *9*, 635−651.
(16) Andreev, Y. G.; MacGlashan, G. S.; Bruce, P. G. *Phys. Rev. B* **1997**, *55*, 12011−12017.
(17) Rietveld, H. M. *J. Appl. Crystallogr.* **1969**, *2*, 65−71.
(18) *Mercury CSD 3.3,* Build RC5; Cambridge Crystallographic Data Centre: Cambridge, U.K., 2013.
(19) Wolff, S. K.; Grimwood, D. J.; McKinnon, J. J.; Turner, M. J.; Jayatilaka, D.; Spackman, M. A. *CrystalExplorer,* Version 3.0; University of Western Australia: Crawley, Australia, 2012.
(20) Zacher, D.; Shekhah, O.; Woll, C.; Fischer, R. A. *Chem. Soc. Rev.* **2009**, *38*, 1418−1429.
(21) Ranjan, R.; Tsapatsis, M. *Chem. Mater.* **2009**, *21*, 4920−4924.
(22) Stock, N.; Biswas, S. *Chem. Rev.* **2012**, *112*, 933−969.
(23) Kartha, V. B.; Venkateswaran, S. *Spectrochim. Acta* **1981**, *11*, 927−934.

DOI: 10.1021/ic5027637
Inorg. Chem. 2015, 54, 2638−2642